High resolution muon tracking with resistive plate chambers

2012 JINST 7 P11018

(http://iopscience.iop.org/1748-0221/7/11/P11018)

PUBLISHED BY IOP PUBLISHING FOR SISSA MEDIALAB

RECEIVED: *July 30, 2012*
ACCEPTED: *October 11, 2012*
PUBLISHED: *November 19, 2012*

SPECIAL ISSUE ON RESISTIVE PLATE CHAMBERS AND RELATED DETECTORS RPC2012

High resolution muon tracking with resistive plate chambers

P. Baesso,[a,1] D. Cussans,[a] J. Davies,[a] P. Glaysher,[a] C. Thomay,[a] C. Vassallo,[a] J. Velthuis,[a] S. Quillin,[b] S. Robertson[b] and C. Steer[b]

[a] *University of Bristol,*
Senate House, Tyndall Avenue, Bristol BS8 1TH, U.K.
[b] *Atomic Weapon Establishment,*
Aldermaston, Reading, RG7 4PR, U.K.

E-mail: paolo.baesso@bristol.ac.uk

ABSTRACT: Following their introduction in the physics community in the early '80s the use of Resistive Plate Chambers (RPCs) as charged particles detectors has constantly increased. Low cost per unit area, good time resolution and easy of operation are some of the features that contributed to such large adoption and that make RPCs interesting for several applications not necessarily related to physics. We built a prototype detector to track cosmic muons and exploit the information provided by estimating the multiple coulomb scattering angle to determine the type of materials they traversed. Simulations show that the technique could be used to inspect a cargo container in a time of the order of minutes.

The detector we built consists of six planes, each one providing X-Y readout over a 50 cm $\times$ 50 cm area. The readout scheme we adopted, based on multiplexing chips used in high energy physics, allowed us to use a limited amount of electronic output channels while still obtaining a spatial resolution lower than 1 mm. An overview of the detector and of the analysis performed on the data is provided.

KEYWORDS: Gaseous detectors; Gaseous imaging and tracking detectors; Particle tracking detectors (Gaseous detectors)

[1] Corresponding author.

doi:10.1088/1748-0221/7/11/P11018

2012 JINST 7 P11018

Contents

2012 JINST 7 P11018

1 Introduction

Resistive Plate Chambers (RPCs) [1] are gaseous detectors widely used in both astrophysics and high energy physics experiments. Among the main features of RPCs are their high detection efficiency for charged particles, their ease of production and operation and their low cost per unit area which, united to the fact that they can be easily scaled up, make RPCs excellent detectors to cover large surfaces. The spatial information provided by RPCs is generally less accurate than that achievable with other detectors but sub-millimeter resolution is achievable with RPCs provided they are operated and readout opportunely [2, 3]. All these features captured the interest of the scientific community even in fields not strictly connected with physics research and there are several examples of studies to exploit RPC technology in applications such as medical imaging [4], geological imaging [5] or homeland security, where there is the need for large areas of detection and where the spatial resolution achieved by RPCs would be sufficient.

In collaboration with the Atomic Weapon Establishment we have built a prototype scanner based on glass RPCs to provide 3D tracking of cosmic muons. The aim of the project is to use the information on the scattering angle for several muon tracks to determine the content of the volume within the detector and to highlight the presence of high-Z materials. Muon Scattering Tomography (MST) has already been discussed in works based on simulated data [6] and first results using large scale prototypes [7] confirm the feasibility of this technique.

In order to use a detector to perform MST an angular resolution of ~ 10 mrad is required if one wants to discriminate between mid-Z materials, like iron, and high-Z materials, such as uranium [8]. The angular resolution can be improved by increasing the distance between the detection layers but this would lead to a reduction in the muon angular acceptance, which would have to be compensated by increasing the detectors area and thus resulting in the system occupying larger volumes and becoming unpractical. For this reason a spatial resolution lower than 1 mm is required, so that the detection layers can be placed at distances of the order of 10 cm.

The results obtained with the current setup are reported here with a particular emphasis regarding the measured spatial resolution and the readout scheme we adopted to reduce the readout costs of the detector.

Figure 1. Frontal view of the prototype setup. The six aluminum cassettes are divided in two groups separated by a gap to insert test materials. The gas mixing system is visible on the bottom of the setup.

2 Setup

The basic detector unit in our prototype is a 2 mm float-glass RPC: two sheets of glass measuring 58 cm × 58 cm are glued to a 4 cm wide glass frame, so that the gas gap obtained measures 50 cm × 50 cm × 2 mm. The gas mixture used to perform the tests described in this work is composed of Ar (60%), freon gas R134A (30%) and C_4H_{10} (10%). The adoption of this mixture was mainly dictated by practical reasons and led us to operate the detectors in streamer mode; to achieve a better spatial resolution the RPC should be operated in avalanche mode and we plan to modify the mixture and the high voltage in this respect once we will finish to collect data with the current setup.

The external surfaces of the detector were spray painted with Charleswater Statguard to obtain a surface resistivity of a few $M\Omega/\square$. Given the small number of detectors produced, the coating was applied manually in our laboratory and this lead to fluctuations in the resistivity across different different detectors, from $\sim 10^5$ $\Omega/\square$ to $\sim 10^7$ $\Omega/\square$. These fluctuations directly influence the spatial resolution of the RPC since they affect how the induced signal spreads across the pickup strips [9, 10].

On top of each RPC sits a printed circuit board which hosts 330 readout strips with 1.5 mm pitch: the strips pick up the signal induced by the charge avalanche produced within the gas chamber. Once all the dead areas on the detector are taken into account, the actual sensitive area remaining measures approximatively 50 cm × 50 cm. The system is comprised of twelve RPCs, hosted in six aluminium cassettes to provide X-Y readout. The cassettes slide into a cabinet which provides mechanical support and allows the spacing between detectors to be adjusted; the prototype is shown in figure 1: it is currently set to allow a central gap of ∼ 70 cm, where a standard sized suitcase could be inserted. A schematic representation of the setup is shown in figure 2.

2012 JINST 7 P11018

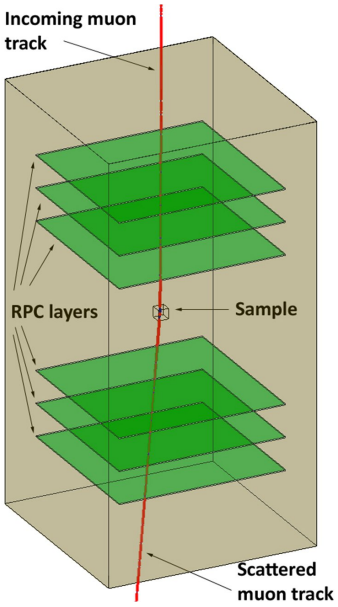

Figure 2. Conceptual representation of the setup: a muon is tracked as it passes through the three top cassettes, scatters within the volume and continues across the bottom cassettes. Each cassette contains two RPCs.

Given the large number of strips to readout we decided to adopt a multiplexing scheme: the signal induced on the strips is fed to a hybrid board supporting four Helix 3.0 chips. The Helix is a family of 0.8 μm CMOS readout chips originally designed for the HERA-B experiment [11] and optimized for silicon microstrip detectors and gaseous chambers. Each chip features 128 analog inputs with programmable shaper and amplifiers and a single analog output. When a trigger is received the four Helix on the hybrid sample the analog value of the strips from one RPC and send them in sequence on a single analog line using a 5 MHz clock. Currently the trigger is provided by two 50 cm $\times$ 50 cm scintillators placed at the top and bottom of the prototype. An external analog-to-digital converter (ADC) is then used to digitize the data; for this we use the commercial CAEN V1724 which also provides clock signals to all the electronics, thus assuring the synchronous operation of the system. By multiplexing the strips we were able to use only 12 ADC channels to read all the 4000 strips of the system. The rate of the cosmic muons is low enough to assure that multiplexing the strips is not causing any loss of data.

3 Data analysis and results

The digitized samples from the RPCs are analyzed by first removing the pedestal and then removing the common-mode contribution. Common mode correction requires particular care: the RPC strips are routed to the Helix in groups of 48 and, because of the differences in cable lengths, each group experiences different grounding and impedance matching, resulting in large regions of strips with different common mode behavior, as shown in figure 3 for a particularly noisy event. Depending on the group of strips, the shape of the common mode offset was found to follow either a first order polynomial or an exponential curve in the form $\alpha - e^{\beta x}$, where x indicates the strip number and α

2012 JINST 7 P11018

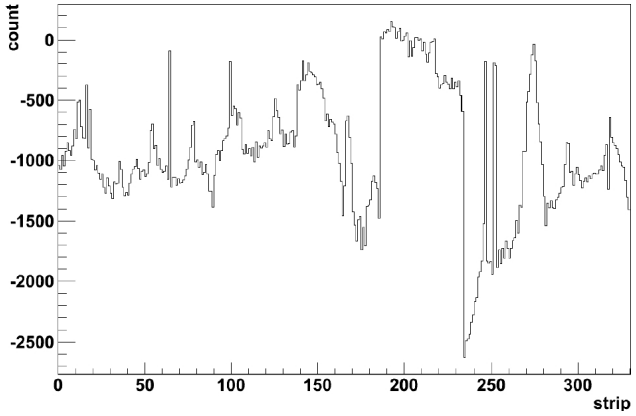

Figure 3. Muon signal in one RPC for a particularly noisy event. The identification of the hit is made difficult by the large fluctuations on some strips.

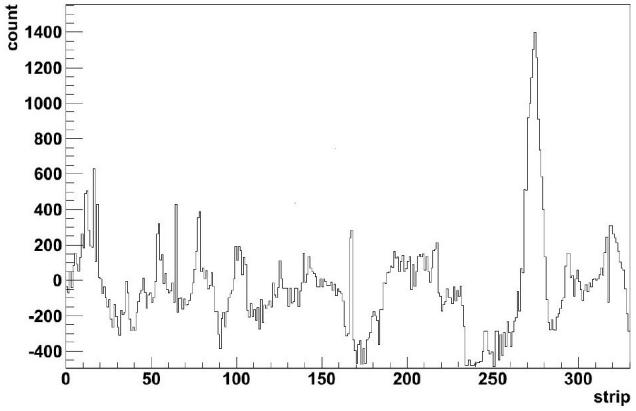

Figure 4. Same signal from figure 3 after pedestal subtraction and common mode correction.

and β are free parameters. This is taken into account by the algorithm which attempts to estimate the common mode parameters and to correct for it on an event-by-event basis; in case of failure the algorithm would simply reject the event. Figure 4 shows the effect of the common mode removal algorithm on the same event of figure 3.

Some of the Helix chips were recovered from a previous experiment and had therefore undergone irradiation and mechanical stress, including having their wire bonds being severed and redone. This is the reason why some of the readout layers show presence of noisy strips and unresponsive channels. The mentioned issues explain the large variation in the signal to noise we measured across the twelve layers, as summarized in table 1.

After the pedestal and common mode are removed, a clustering algorithm is applied to the each layer followed by a gaussian fit of the strips in the cluster, as illustrated in figure 5. Figure 6 shows the cluster size distribution for one of the RPC layers and indicates that the charge profile spreads across a width of ~ 10 mm. By operating the RPCs in avalanche mode it would be possible to reduce the charge profile, therefore obtaining smaller clusters thus increasing the accuracy in the muon position reconstruction.

2012 JINST 7 P11018

Table 1. Signal to noise ratio for the readout layers of the detector. RPC are numbered from 0 to 5 for the X readout and from 6 to 11 for the Y readout. RPC 0 and 6 are installed in the top cassette, 5 and 11 in the bottom one.

Layer	X Readout (S/N)	Layer	Y Readout (S/N)
0	93	6	68
1	58	7	69
2	44	8	47
3	65	9	23
4	31	10	47
5	48	11	54

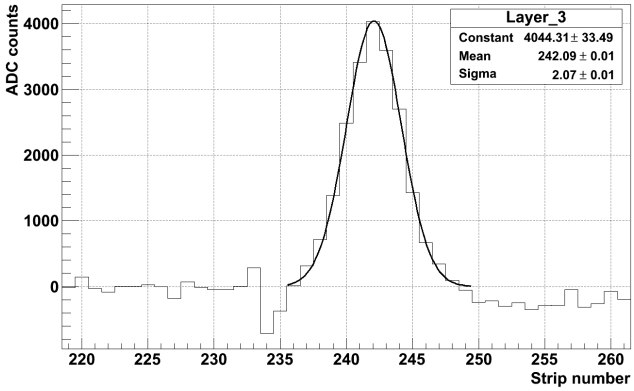

Figure 5. Gaussian fit of the strips to determine the muon hit position on one of the RPC. Fit parameters are provided in the box.

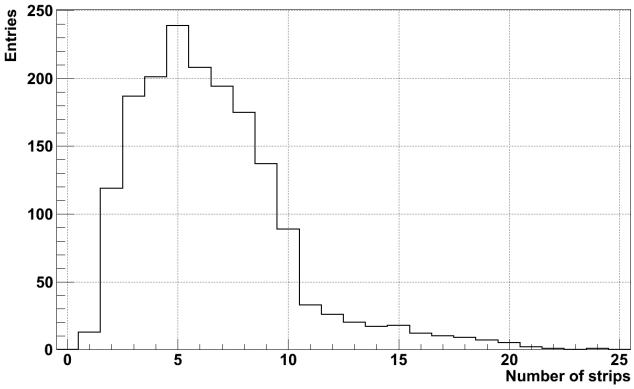

Figure 6. Cluster size distribution for a sample of 1700 muons in one of the RPC layers.

An additional step was also introduced to improve the precision of the hit position: the connection pattern of the strips is such that, due to the cross talk between them, for every actual pulse picked-up by the strips a lower, mirror pulse is produced in a different region of strips (XT pulses). An example of a XT pulse is shown in figure 7. It was found that cross talk peak amplitude is predominantly a fraction of the actual hit signal of around 15%. The expected position of the XT

2012 JINST 7 P11018

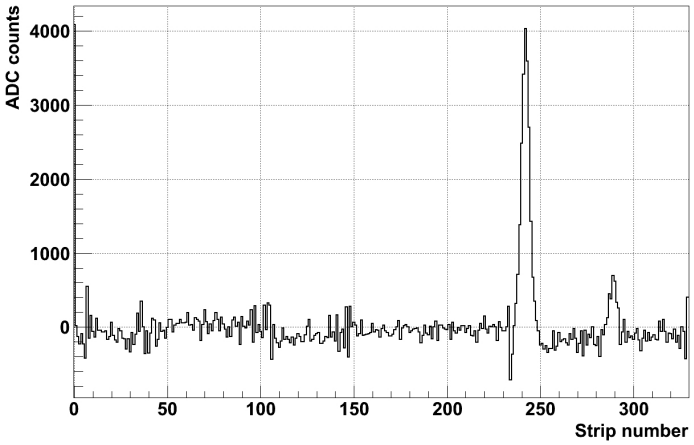

Figure 7. Example of cross talk pulse for one of the RPC: the actual pulse is clearly visible around strip 240 and the lower mirror pulse is near strip 290. The expected relative position between actual pulse and XT pulse is known therefore the XT pulse can be used to discriminate between genuine pulses and noise originated from common mode.

pulses is known, since it only depends on the relative position of the strips within each detector. Events with a ratio between 0.08 and 0.4 (cross talk amplitude/signal amplitude) and whose position corresponded to the expected one were therefore selected as good events with positive cross talk ID. This technique improves the detector resolution but, since the XT pulse was not always easily identified, the number of usable events dropped significantly: the fraction of complete tracks which passed the cut is about 1% of the tracks in the data set.

Figure 8 shows the raw detector resolution, defined as the difference between the reconstructed hit on the RPC layer and the extrapolated hit obtained by performing a track fit without the layer under consideration. The difference in spatial resolution between the layers can be explained by the non homogeneity in the resistive coating, which directly affects the charge profile as mentioned before, and in the hardware performances, with some Helix showing an larger amount of noise.

Once the hit position on each RPC has been determined, the algorithm attempts to fit a straight line across the six cassettes by first performing a linear interpolation of the points in the XZ and YZ projections independently and using a χ^2 cut to reject noisy events. The two projections are then combined in a 3D track; a final cut on the χ^2 value assures that the track is actually due to a single particle and that there are no false hits or multiple hits: with this analysis we managed to achieve a detection efficiency above 99% and a purity better than 95% across the individual layers, using the set of tracks which passed the final χ^2 cut.

In order to determine the resolution of the detector σ a straight line is fit to all except one of the reconstructed hits of an event. The excluded hit is the hit of interest x_{hit} and is compared to the predicted hit position x_{fit} given by the intersect of fit line and detector plane. A residual r is computed for each point of multiple events by $r = x_{\text{hit}} - x_{\text{fit}}$. A histogram of all residuals assumes a gaussian distribution, the standard deviation of which is defined as the resolution σ. While this approach assumes that the muon track is a straight line through the detector, in reality the muon will undergo multiple scattering due to the materials encountered along the path (such as the glass of the RPC, the aluminium of the cassettes, the mechanical supports, etc) therefore what we measure

2012 JINST 7 P11018

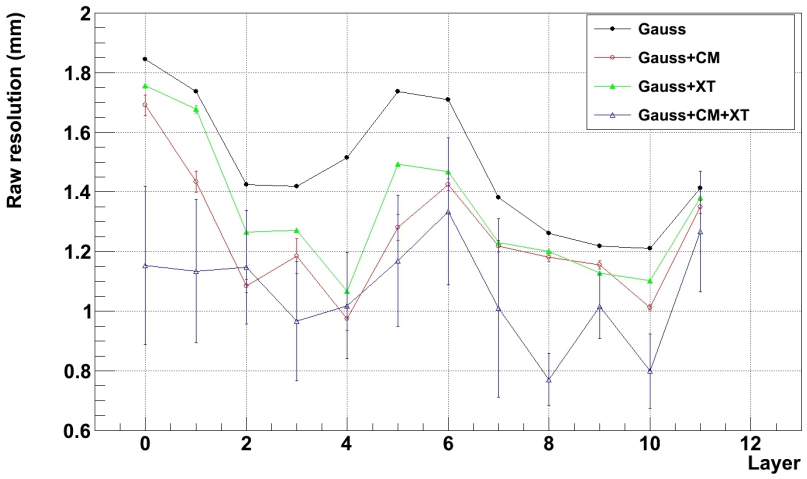

Figure 8. Raw resolution for the twelve RPCs using different hit finding approaches and noise rejection: pure gauss fit (black), gauss fit after common mode rejection (Gauss+CM, shown in red), gauss fit after XT rejection (Gauss+XT, shown in green) and gauss fit with common mode and cross talk rejection (Gauss+CM+XT, shown in blue). While the results with this latest approach are generally better, the statistics decreases significatively, explaining why the relative error increases. The layers are numbered with the same convention adopted for table 1.

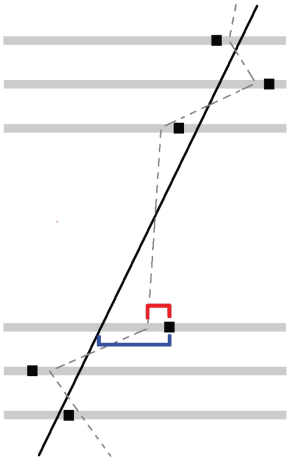

Figure 9. Diagram of a muon path (dashed line), the reconstructed hit positions (black squares) and the fitted track (black line). The raw resolution (blue) is the difference between the linear fit position and the reconstructed hit position while the intrinsic resolution (red) is the difference between the actual hit position and the reconstructed position.

is the raw resolution of the setup σ_{raw}. An exaggerated representation of the difference between raw and intrinsic resolution is provided in figure 9. In order to obtain the intrinsic resolution of each plane σ_{int} we need to extrapolate the contributions due to multiple scattering and geometrical factors from σ_{raw}. We addressed this by using a Geant4 [12] simulation of our setup, where all the materials and the geometry of the detectors were carefully taken into account. To find the intrinsic resolution of the detector system, a range of intrinsic resolutions were modeled in the simulation and the resulting data output was compared to experimental data. The intrinsic resolution was

2012 JINST 7 P11018

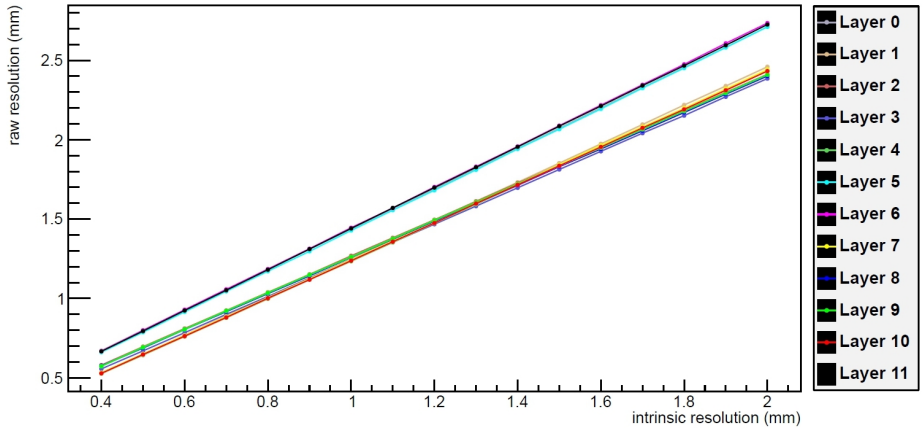

Figure 10. Raw resolution versus intrinsic resolution expected from Monte Carlo simulation for all 12 RPC layers. Two distinct groups appear: the upper set of lines (layers 0, 5, 6 and 11) correspond to all the outer planes, and the lower set of lines correspond to all the inner planes.

introduced into the Monte Carlo by smearing RPC hit points with a gaussian of corresponding standard deviation. A range of intrinsic resolutions from 0.4 mm to 2 mm were investigated and for each modeled resolution the simulation was run for one million muon events with approximately 30,000 of these fully traversing the detector. The resulting hit position data was analyzed in the same way as experimental data: tracks were fitted and residuals where calculated, giving a raw resolution for each RPC. Figure 10 shows the results of the Geant4 simulation, illustrating how the intrinsic resolution of each detector is worsened by the geometrical and scattering contributions: for each value of intrinsic resolution, used as a starting point, the simulation estimates the resulting raw resolution of the layer. Taking into consideration figure 8 and figure 10 the resulting intrinsic resolution for the layers is generally within 0.6 mm (layer 8 and 10) and 1 mm (layer 6) with most of the layers having a resolution close to 0.8 mm.

The information on the hit position on each layer is used to produce two tracks, one relative to the top half of the detector and one to the bottom half and to estimate the scattering angle between the two tracks. The detector volume is then divided into voxels and populated according to the number of tracks which scatter within it with an angle greater than 0.03 radians. This is a very simple approach and does not make full use of tomography techniques since it discards many informations contained in the tracks (for instance there is no weight on the actual scattering angle). However, it is sufficient to prove the correct behavior of the prototype and of the data analysis tools. To test it we placed a block of lead sized 10 cm $\times$ 10 cm $\times$ 15 cm within the scanner volume and analyzed the data obtained. Figure 11 shows a preliminary analysis of the data after $\sim$ 100 minutes of acquisition: the centers with scattering angles greater than 0.03 radians are concentrated in the area where we placed the lead block. The long time for this acquisition was chosen to be able to visually identify the lead block and verify the correct positioning within the volume but this approach is not viable for a practical application of the detector. A more sophisticated analysis, not presented here, is currently being developed by our group and shows that the data obtained with the detector can be used to classify a target sample as "*threat*" or "*no-threat*" within a few minutes of data taking [13]. In this case the aim is not to image the volume but to determine if the

2012 JINST 7 P11018

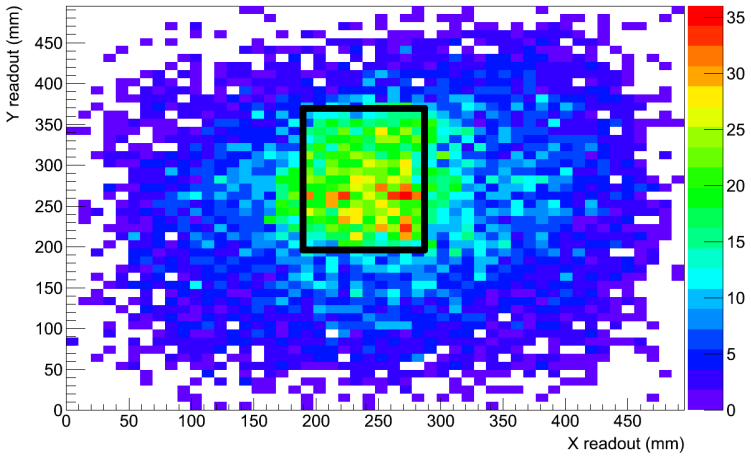

Figure 11. Imaging of a 10 cm × 10 cm × 15 cm lead block placed within the detector. The image is obtained using 10000 events and populating only those voxels where the scattering angle is greater than 30 mrad. The position of the lead block is indicated by the black square.

scattering angle distribution is compatible with the presence of high-Z materials anywhere within the volume: this is done by producing a numerical value which indicates the likelihood of having any suspicious material within the detector.

4 Conclusions

We described a muon tracker based on resistive plate chambers and multiplexing readout chips and provided an overview of its main features, with particular emphasis on the spatial resolution, proving that it is better than 1 mm across all the detectors. The non uniform response across the layers can be explained in term of manufacturing process of the RPCs and of the noise on the readout electronic. The spatial resolution could be further improved by operating the detectors in avalanche rather than streamer mode and we plan to do this in our future studies.

We also described the analysis performed on the data collected so far, including simulations with Geant4 and actual events. The quality of the data is affected by the noise in the readout electronics which, in the current setup, can be addressed by performing cuts based on the several technique even if this reduces the amount of usable data. To improve this aspect of the project we are currently implementing the readout hardware based on new multiplexing chips.

In order to verify the correct behavior of the detector and the data analysis code we created the image of a lead block by simply plotting the tracks with high scattering angles, using data collected over about two hours. A much faster and refined analysis is being developed within our group and shows that minute-equivalent data acquisitions can be enough to positively identify lead. In this scenario a container could be scanned for one or two minutes and the data would be analyzed to produce a “risk indicator” which would be used to determine whether the cargo is safe or should be subject to further and more accurate inspection.

2012 JINST 7 P11018

References

[1] R. Santonico and R. Cardarelli, *Development of resistive plate counters*, *Nucl. Instrum. Meth.* **187** (1981) 377.

[2] E. Ceron Zeballos et al., *Resistive plate chambers with secondary electron emitters and microstrip readout*, *Nucl. Instrum. Meth.* **392** (1997) 150.

[3] Q. Li et al., *Study of spatial resolution properties of a glass RPC*, *Nucl. Instrum. Meth.* **A 663** (2012) 22.

[4] I. Torres-Espallardo et al., *Simulation study of resistive-plate-chambers based PET for hadron-therapy monitoring*, *IEEE Nucl. Sci. Symp. Conf. Rec.* (2011) 3529.

[5] TOMUVOL collaboration, C. Carlogânu, *Density imaging of volcanoes with atmospheric muons using GRPCs*, in Proceedings of the *XXI International Europhysics Conference on High Energy Physics*, Grenoble France, 21–27 Jul 2011 [PoS(EPS-HEP2011)055].

[6] L.J. Schultz et al., *Statistical reconstruction for cosmic ray muon tomography*, *IEEE T. Image Process.* **16** (2007) 1985.

[7] S. Pesente et al., *First results on material identification and imaging with a large-volume muon tomography prototype*, *Nucl. Instrum. Meth.* **A 604** (2009) 738.

[8] L. Cox et al., *Detector requirements for a cosmic ray muon scattering tomography system*, *Nucl. Sci. Symp. Conf. Rec.* (2008) 706.

[9] W. Riegler and C. Lippmann, *The physics of resistive plate chambers*, *Nucl. Instrum. Meth.* **A 518** (2004) 86.

[10] Y. Jin et al., *Studies on RPC position resolution with different surface resistivity of high voltage provider*, *Nucl. Sci. Symp. Conf. Rec.* (2008) 917.

[11] ZEUS collaboration, *The design and performance of the ZEUS micro vertex detector*, *Nucl. Instrum. Meth.* **A 581** (2007) 656 [arXiv:0708.3011].

[12] GEANT4 collaboration, *Geant4 — a simulation toolkit*, *Nucl. Instrum. Meth.* **A 506** (2003) 250, software release: 4.9.4 p02.

[13] C. Thomay et al., *A novel technique to detect special nuclear material using cosmic rays*, talk given at the *IEEE 2012 Nuclear Science Symposium and Medical Imaging Conference*, Anaheim U.S.A., 29 Oct–3 Nov 2012.

2012 JINST 7 P11018